Frequency decoding of periodically timed action potentials through distinct activity patterns in a random neural network

2012 New J. Phys. 14 113022

(http://iopscience.iop.org/1367-2630/14/11/113022)

New Journal of Physics
The open access journal for physics

Frequency decoding of periodically timed action potentials through distinct activity patterns in a random neural network

Tobias Reichenbach and A J Hudspeth[1]

Howard Hughes Medical Institute and Laboratory of Sensory Neuroscience, The Rockefeller University, New York, NY 10065, USA
E-mail: hudspaj@rockefeller.edu

New Journal of Physics **14** (2012) 113022 (17pp)
Received 10 July 2012
Published 20 November 2012
Online at http://www.njp.org/
doi:10.1088/1367-2630/14/11/113022

Abstract. Frequency discrimination is a fundamental task of the auditory system. The mammalian inner ear, or cochlea, provides a place code in which different frequencies are detected at different spatial locations. However, a temporal code based on spike timing is also available: action potentials evoked in an auditory-nerve fiber by a low-frequency tone occur at a preferred phase of the stimulus—they exhibit phase locking—and thus provide temporal information about the tone's frequency. Humans employ this temporal information for discrimination of low frequencies. How might such temporal information be read out in the brain? Here we employ statistical and numerical methods to demonstrate that recurrent random neural networks in which connections between neurons introduce characteristic time delays, and in which neurons require temporally coinciding inputs for spike initiation, can perform sharp frequency discrimination when stimulated with phase-locked inputs. Although the frequency resolution achieved by such networks is limited by the noise in phase locking, the resolution for realistic values reaches the tiny frequency difference of 0.2% that has been measured in humans.

[1] Author to whom any correspondence should be addressed.

Contents

1. Introduction

A sound impinging on the eardrum elicits a wave of displacement of the basilar membrane within the cochlea [1, 2]. Mechanosensitive hair cells on the basilar membrane transduce the membrane's vibration into electrical signals that are transmitted to the associated auditory-nerve fibers [3, 4]. Through position-dependent resonance along the basilar membrane the cochlea establishes a place code for frequencies. Stimulation at a high frequency evokes a traveling wave that peaks near the organ's base. The waves elicited by lower frequencies culminate at more apical positions.

A temporal code may, however, supplement or even supersede the place code. In response to a pure tone at a frequency below about 300 Hz, an auditory-nerve fiber fires action potentials at every cycle of stimulation and at a fixed phase [3, 5]. Above 300 Hz the axon starts to skip cycles, but action potentials still occur at a preferred phase of the stimulus. The quality of this phase locking decays between 1 kHz and 4 kHz, however, and phase locking is lost for still higher frequencies. Phase locking below 4 kHz is sharpened in the auditory brainstem by specialized neurons such as spherical bushy cells that receive input from multiple auditory-nerve fibers [6, 7]. These cells can fire action potentials at every cycle of stimulation up to 800 Hz (figure 1). Temporal information about the stimulus frequency is therefore greatest for frequencies below 800 Hz, declines from 800 Hz to 4 kHz, and vanishes for still greater frequencies. In some species, such as the barn owl, phase locking can continue up to 10 kHz [8].

Phase locking is employed for sound localization in the horizontal plane [9, 10]. A sound coming from a subject's left, for example, reaches the left ear first and hence produces a phase delay in the stimulus at the right ear compared to that at the left. Auditory-nerve fibers preserve this phase difference, which is subsequently read out by binaurally sensitive neurons through delay and coincidence detection. A temporal delay generally results when one neuron signals another: the signal propagates along the axon of the transmitting neuron and along the dendrites of the receiving cell, producing delays of up to 20 ms with only a few microseconds of jitter [11–13]. Coincidence detection occurs when two or more synchronous incoming spikes are required for a neuron to fire: the signals must arrive at the nerve cell's soma within a certain time window τ, comparable to the membrane's time constant, in order for their effects to add and initiate an action potential.

Phase locking can also provide information about the frequency of a pure tone, for the duration between two successive neural spikes is on average the signal's period or a multiple

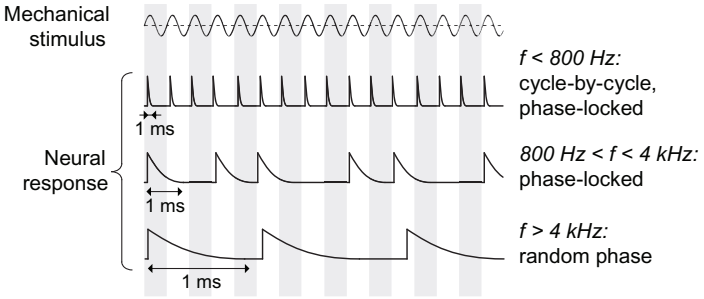

Figure 1. Schematic illustrations of phase locking. A stimulus at a frequency below 800 Hz elicits a series of action potentials in, for example, spherical bushy cells of the auditory brain stem; spikes occur at every cycle of stimulation and at a preferred phase. Because an action potential lasts about 1 ms, those neurons no longer fire spikes at every cycle when the signal frequency exceeds 800 Hz. Spikes still occur, however, at a preferred phase. Above 4 kHz the spikes' phases are random.

thereof. Evidence for the usage of this information in the brain comes from psychoaoustic studies showing that human frequency discrimination is superior for the lower frequencies at which phase locking is available and that discrimination of these frequencies worsens when the phase information is perturbed [14–18].

It remains unclear how the temporal information on frequency is read out in the brain. The usage of delay and coincidence detection has been proposed, but the exact mechanism has not been specified and the resulting frequency resolution has not been determined [19]. Other studies have advanced mathematical schemes for determining a signal's frequency from phase locking, the neural implementation of which remains unclear [20, 21]. Here we study how a random recurrent neural network with delay and coincidence detection can encode frequency in its activity pattern when stimulated with phase-locked, cycle-by-cycle input. We develop a statistical description of these firing patterns and show that they provide precise frequency information.

2. Results

Denote by T the period and by L the duration in cycles of a signal such that the phase-locked, cycle-by-cycle external spikes arrive at the network neurons around times $0, T, 2T, 3T, \ldots, (L-1)T$ (figure 2). Assume that the first external spike triggers an action potential at each neuron; because of adaption, two coincident spikes are needed for the generation of subsequent spikes. If a neuron i projects to another neuron j then its first spike arrives there at a later time t_{ij} that represents the delay between the cells. If that time differs no more than the small amount τ from the time T at which the second external spike arrives at neuron j, the two spikes act in concert to elicit an action potential; otherwise neuron j remains silent. If active, neuron j may trigger spikes in other neurons, specifically those for which the time delay from neuron j also matches the signal period. Sustained network activity results when the connectivity C between neurons—the average number of internal connections that a neuron receives—exceeds a certain value (figure 3; appendices A and B).

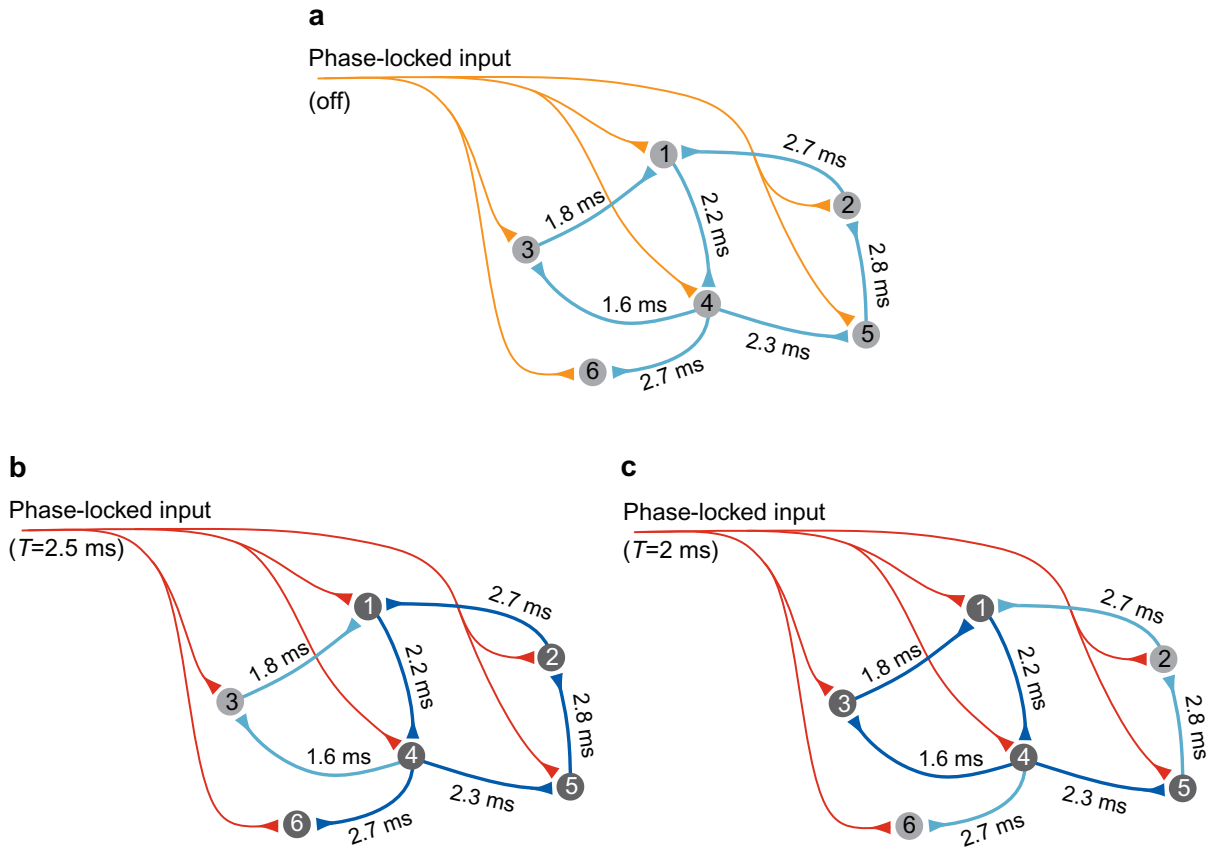

Figure 2. Schematic diagrams of a neural network with delay and coincidence detection. (a) Each neuron (light gray) can receive phase-locked inputs from a preceding neuron through external nerve fibers (orange). The network neurons are randomly connected (light blue) with the indicated characteristic delays in signal propagation. To fire an action potential, a neuron requires two temporally coincident spikes, such as one from an external and one from an internal source. (b) When a periodic signal arrives through the external nerve fibers (red), the internal connections whose signal delay is approximately matched to the signal period induce spikes in their target neurons, resulting in a pattern of active internal connections (dark blue) and active neurons (dark gray). (c) A different signal period evokes a distinct pattern of active connections and active neurons.

How can we quantify this network's pattern of activity? Let the network comprise N neurons and denote a neuron as active if it fires spikes in response to at least half of the external spikes and as inactive otherwise. The network's activity may then be summarized by a binary vector $\boldsymbol{x}_T = (x_T^{(1)}, x_T^{(2)}, \ldots, x_T^{(N)})$ in which $x_T^{(i)} = 1$ if neuron i ($i = 1,\ 2, \ldots, N$) is active under stimulation at a period T and 0 otherwise. The fraction a of active nodes follows as

$$a = N^{-1} \sum_{i=1}^{N} x_T^{(i)}. \tag{1}$$

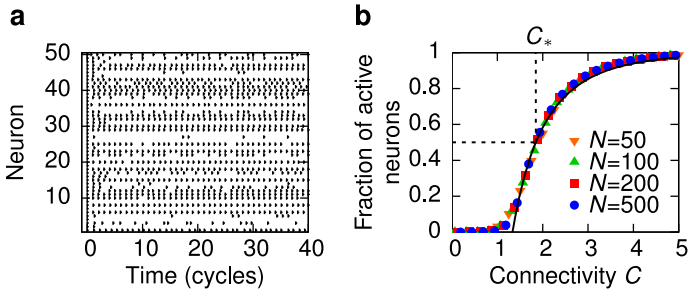

Figure 3. Patterns of network activity. (a) Each horizontal line depicts the activity of a single neuron in the network. Because every cell fires a spike upon receiving the first input signal, the raster of action potentials displays a vertical black line at its outset. The generation of spikes subsequently requires two incoming action potentials that temporally coincide. The connections between neurons induce different delays, so an activity pattern results in which some neurons fire at almost every cycle whereas others remain silent. Noise in the timing of the external spikes introduces variation in the firing of each neuron. (b) The fraction of active neurons depends on the mean connectivity C, the average number of internal connections that each neuron receives. An analytical approximation (black line) confirms that the fraction of active neurons is independent of the network size N. Half of the neurons are active at a connectivity C_*.

An analytical approximation provides insight into the dependence of the network's activity on its connectivity and size. Assume that a neuron j is active if it receives at least one active connection, in which we define a connection from another neuron i to neuron j as active if spikes from neuron i traveling to neuron j can elicit action potentials there in at least half of the trials. Denote the average number of active connections that a neuron receives by B. The probability that a neuron does not receive any active connection then reads $[1 - B/(N-1)]^{a(N-1)}$ and equals the fraction of inactive neurons:

$$1 - a = [1 - B/(N-1)]^{a(N-1)} \approx \mathrm{e}^{-aB}. \tag{2}$$

The approximation can be solved through the Lambertz W-function

$$a = 1 + \frac{1}{B} W(-B\mathrm{e}^{-B}). \tag{3}$$

Further analysis shows that the average number of active connections can be approximated as $B = 2\tau C/(t_{\max} - t_{\min})$ and the analytically derived average network activity is then in excellent agreement with numerical simulations (figure 3(b) and appendix B). The fraction of active nodes does not depend on the network size N if the network connectivity C is independent of N. Because the probability c of a connection between two neurons follows as $c = C/(N-1)$ the resulting network is sparse.

Below we will show that stimulation at different periods T leads to different activity patterns with the same mean activity a. How much information on the signal period can one individual activity pattern contain? The potential information content follows from the number of combinatorial possibilities that exist for activity patterns with the same mean activity a. More specifically, the more possibilities for such patterns, the higher the information content of each. Basic combinatorics informs us that a mean activity of $a = 1/2$, which implies that half of

the neurons are active and the remaining half inactive, allows the greatest number of activity patterns. Those patterns are hence the most informative. As the other extreme cases, the mean activities $a = 0$ and 1 can each be realized through only one corresponding activity pattern and each accordingly contains no information on the signal period. We denote the network connectivity at which half of the neurons are active by C_* and employ it in the following.

Inaccuracy in phase locking results in noise: spikes from spherical bushy cells, for example, exhibit a phase distribution that is approximately Gaussian around the mean value with a standard deviation s that can be as small as one-twentieth of a cycle [7]. Input spikes therefore arrive at the network neurons at times $\xi_1, T + \xi_2, \ldots, (L-1)T + \xi_L$ in which ξ_k $(k = 1, 2, \ldots, L)$ is a random Gaussian variable with zero mean and standard deviation s. Although small, this noise evokes slightly different neural activity patterns upon repeated stimulation. We define this mean pattern as $\boldsymbol{X}_T = (X_T^{(1)}, X_T^{(2)}, \ldots, X_T^{(N)})$ in which $X_T^{(i)} = 1$ if neuron i $(i = 1, 2, \ldots, N)$ is active in at least half of the trials and $X_T^{(i)} = 0$ otherwise.

Stimulation at another signal period T' evokes a different mean activity pattern $\boldsymbol{X}_{T'}$. We can quantify its difference from the mean pattern $\boldsymbol{X}_T$ at period T through the relative Hamming distance between the patterns:

$$d(\boldsymbol{X}_T, \boldsymbol{X}_{T'}) = \frac{1}{N} \sum_{i=1}^{N} |X_T^{(i)} - X_{T'}^{(i)}|. \tag{4}$$

This distance specifies the fraction of neurons that differ in their activity between the two patterns. Analytical calculations and numerical simulations show that the distance increases linearly in the absolute period difference $|T' - T|$ and vanishes for $T' = T$ (figure 4(a) and appendix C). The network thus decodes stimulation periods through distinct patterns of mean activity. Each such pattern may then selectively activate a particular downstream neuron, whose activity encodes a specific frequency of stimulation.

The identification of the period from an individual signal is inevitably limited by the noise in the timing of the external spikes. When a network is stimulated at a period T its single-trial activity pattern $\boldsymbol{x}_T$ differs both from the mean pattern $\boldsymbol{X}_T$ at period T and from the mean pattern $\boldsymbol{X}_{T'}$ at another period T'. Correct discrimination between T and T' thus requires the pattern $\boldsymbol{x}_T$ to be closer to $\boldsymbol{X}_T$ than to $\boldsymbol{X}_{T'}$.

The relative Hamming distance $d(\boldsymbol{x}_T, \boldsymbol{X}_T)$ between $\boldsymbol{x}_T$ and $\boldsymbol{X}_T$ is the average over the N random variables $|x_T^{(i)} - X_T^{(i)}|$. An analytical approximation shows that these variables can be regarded as effectively independent. The distribution of $d(\boldsymbol{x}_T, \boldsymbol{X}_T)$ is therefore Gaussian around a mean value $D(\boldsymbol{x}_T, \boldsymbol{X}_T)$ with a certain standard deviation σ (figure 4(b) and appendix C). The distance $d(\boldsymbol{x}_T, \boldsymbol{X}_{T'})$ between $\boldsymbol{x}_T$ and $\boldsymbol{X}_{T'}$ is also Gaussian around another mean value $D(\boldsymbol{x}_T, \boldsymbol{X}_{T'})$ but with the same standard deviation σ as for $d(\boldsymbol{x}_T, \boldsymbol{X}_T)$ (figure 4(d)). The two distributions can be differentiated with at least 95% accuracy when the mean values $D(\boldsymbol{x}_T, \boldsymbol{X}_T)$ and $D(\boldsymbol{x}_T, \boldsymbol{X}_{T'})$ differ by 4σ or more. When is this condition fulfilled?

Because larger system sizes N imply averaging over more neurons, and as confirmed by analytical and numerical computations, the standard deviation σ decreases as $N^{-1/2}$ in accordance with the central limit theorem (figure 4(c) and appendix C). We can therefore resort to a network that is large enough to yield a sufficiently small variance in the relative Hamming distance. Correct discrimination of a signal's period between T and T' is then feasible as soon as the mean value $D(\boldsymbol{x}_T, \boldsymbol{X}_T)$ is distinct from $D(\boldsymbol{x}_T, \boldsymbol{X}_{T'})$.

How does the mean value $D(\boldsymbol{x}_T, \boldsymbol{X}_{T'})$ depend on the difference in periods? Analytical and numerical computations show that $D(\boldsymbol{x}_T, \boldsymbol{X}_{T'})$ increases linearly in $|T' - T|$ when

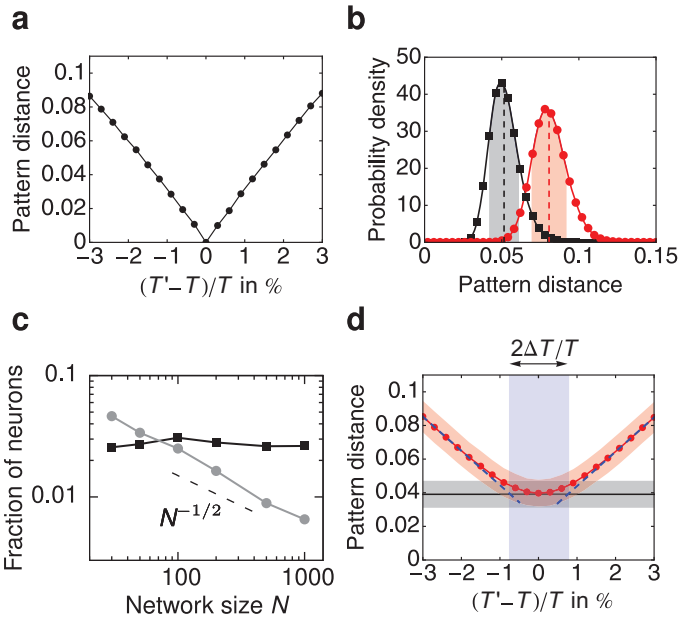

Figure 4. Distances of activity patterns evoked by different signal periods. (a) The average distance between the mean activity pattern for period T and that for period T' increases linearly in the absolute value $|T' - T|$ of the period difference. Here we have employed $N = 1000$ and $L = 100$. (b) The distributions of the distances $d(\boldsymbol{x}_T, \boldsymbol{X}_T)$ (black squares) and $d(\boldsymbol{x}_T, \boldsymbol{X}_{T'})$ (red circles) are approximately Gaussian around the mean values $D(\boldsymbol{x}_T, \boldsymbol{X}_T)$ (dashed black line) and $D(\boldsymbol{x}_T, \boldsymbol{X}_{T'})$ (dashed red line). This result has been obtained from a single network with $N = 1000$ neurons, a signal of $L = 10$ cycles, and $(T - T')/T = 3\%$. Averaged over multiple networks, the standard deviation σ (shading) is equal for the two configurations. (c) The mean value $D(\boldsymbol{x}_T, \boldsymbol{X}_T)$ (black squares) is independent of the network size N, whereas the standard deviation σ (gray circles) decreases for larger N. The results were obtained for a signal of length $L = 50$ cycles. (d) The dependence of the distribution of $d(\boldsymbol{x}_T, \boldsymbol{X}_{T'})$ on the period difference $|T' - T|$ is plotted for $N = 300$ and $L = 20$. The mean value $D(\boldsymbol{x}_T, \boldsymbol{X}_{T'})$ (red circles) has a minimum for $T' = T$, at which it reaches $D(\boldsymbol{x}_T, \boldsymbol{X}_T)$ (horizontal black line). For $|T' - T|$ above a threshold value ΔT the mean value $D(\boldsymbol{x}_T, \boldsymbol{X}_{T'})$ increases linearly in $|T' - T|$ (dashed blue line), whereas it exhibits a quadratic dependence below (blue shading). The standard deviation σ of $d(\boldsymbol{x}_T, \boldsymbol{X}_{T'})$ (red shading) does not depend on the period difference and equals the standard deviation of $d(\boldsymbol{x}_T, \boldsymbol{X}_T)$ (gray shading).

$|T' - T| > \Delta T$ for a threshold difference ΔT (figure 4(d) and appendix C). When the periods of the two signals are closer, $|T' - T| < \Delta T$, the distance $D(\boldsymbol{x}_T, \boldsymbol{X}_{T'})$ is proportional to the squared period difference $(T' - T)^2$ and approaches $D(\boldsymbol{x}_T, \boldsymbol{X}_T)$ for $T' = T$. The threshold ΔT thus provides a measure for the smallest period difference that a particular network can resolve.

The threshold value ΔT is proportional to the mean distance $D(\boldsymbol{x}_T, \boldsymbol{X}_T)$ between a single-trial pattern $\boldsymbol{x}_T$ and the mean pattern $\boldsymbol{X}_T$ at period T (figure 5 and appendix C). Because the pattern evoked by a signal of greater length L involves more averages over external spike times,

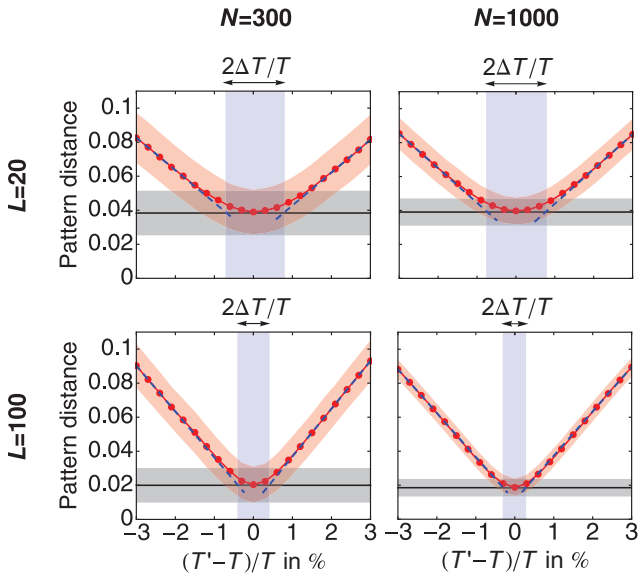

Figure 5. Influence of network size N and signal length L. The mean distance $D(\boldsymbol{x}_T, \boldsymbol{X}_{T'})$ (red circles) does not change with increasing N but the standard deviation (red shading) is progressively reduced. Longer signals, however, induce a lower mean value $D(\boldsymbol{x}_T, \boldsymbol{X}_T)$ (black line) and hence a smaller value ΔT at which the crossover occurs from linear to quadratic dependence of $D(\boldsymbol{x}_T, \boldsymbol{X}_{T'})$ on $|T' - T|$ (blue shading). The standard deviations of $d(\boldsymbol{x}_T, \boldsymbol{X}_{T'})$ (red shading) and $d(\boldsymbol{x}_T, \boldsymbol{X}_T)$ (gray shading) also decline for longer signals.

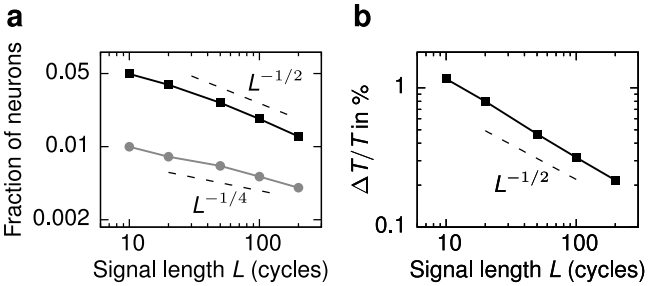

Figure 6. Dependence of period resolution on signal length L. (a) The mean value $D(\boldsymbol{x}_T, \boldsymbol{X}_T)$ (black squares) decreases as $L^{-1/2}$ with increasing signal length whereas the standard deviation σ (gray circles) exhibits the weaker dependence $L^{-1/4}$. The results were computed for $N = 1\,000$. (b) The period resolution ΔT achieved by a network with $N = 500$ also decreases as $L^{-1/2}$.

and hence over the phase noise, it results in a mean value $D(\boldsymbol{x}_T, \boldsymbol{X}_T)$ that decreases as $L^{-1/2}$ (figure 6(a) and appendix C). However, a larger network size N does not affect $D(\boldsymbol{x}_T, \boldsymbol{X}_T)$ (figures 4(c) and 5).

The threshold ΔT also decreases as $L^{-1/2}$ with increasing signal length L (figure 6(b)). Longer signals indeed provide more information that can enhance frequency resolution. The improvement in resolution is less than that expected from the Fourier uncertainty principle, in which frequency resolution is inversely proportional to signal length [22].

The threshold ΔT for a given signal length is proportional to the noise in the phase-locked input signal but independent of the neural network's parameters (appendix C). For a realistic value for the standard deviation s of one-twentieth of a cycle and for a signal of length $L = 200$ cycles, we obtain a period resolution $\Delta T/T$ of about 0.2% (figure 6(b)). This value agrees well with the human frequency resolution measured in psychoacoustic experiments [15].

3. Discussion

When the brain employs the temporal information contained in phase locking, does it need to translate the temporal code into another one such as the population code considered here, or could it leave the temporal representation as it is? We believe that at some point the brain must translate the temporal information—possibly integrated with other information—into the activity of relatively few specific 'grand-mother' neurons. Indeed, in a psychoacoustic task of frequency discrimination, human subjects transform their perception of the comparative frequencies of two tones into motion activity of their hands and fingers through which they interact with a computer to communicate their judgment. Such motion is controlled by the sparse activity of a few motor neurons.

Here we propose a mechanism for how the temporal information on frequency can be encoded in the activity pattern of a neuronal population. A simple, randomly connected network with a range of signal-propagation delays between neurons can use phase-locked inputs to replicate the striking frequency discrimination of the human auditory system. As we discuss below, the population code may then be transformed at a second stage into a representation through single-neuron activity.

The network encodes different input frequencies in distinct activity patterns. We have defined those patterns in the simplest possible way, through the mean activity of the network's neurons during stimulation. Further statistics of the spike trains fired by the neurons, such as temporal correlation between the spikes from individual neurons and correlation between spikes from different neurons, could lead to finer discrimination of activity patterns and hence improve the precision of frequency discrimination.

The population code that we have defined here may be read out by downstream neurons. A given downstream neuron may detect a particular activity pattern of the network if it receives excitatory connections from the neurons that are active for this pattern and inhibitory connections from the neurons that are inactive for this pattern. Such a representation may be learned through reinforcement of the excitation as well as the inhibition upon activity of the corresponding network neurons. The properties and precision of such a downstream read-out will be investigated in future studies.

Frequency resolution is limited by noise. Here we have considered jitter in the phase-locked input. The time delays employed by the network, however, arise through the conduction of action potentials along axons and are also subject to fluctuations. Experimental as well as simulation studies show that the standard deviation for fluctuations in action-potential velocity is typically below 1% [12, 23]. In contrast, the noise in phase locking has standard deviations of a few per cent or more of the signal's period T. We have therefore ignored fluctuations in conduction velocity, which may be the subject of a future study.

Temporal delays may also vary on longer time scales. Variation in body temperature can alter synaptic delays [24]. Aging can change axonal myelination, for example, and thereby conduction delays. Such changes may be compensated by other variations in axonal conduction

velocity or synaptic transmission such that the frequency-specific activity patterns remain the same. Alternatively, if the activity patterns were to change, their read-out through downstream 'grand-mother' neurons might adapt appropriately through learning.

In our simulations we have employed a range of temporal delays between network neurons that encompasses about an octave. Frequency discrimination by such a network is accordingly restricted to a spectral band of less than an octave, so many networks, each with a distinct range of temporal delays, are required to cover a broader frequency range. Where might such structures exist in the brain? The inferior colliculus displays a tonotopic array of multiple frequency-band laminae, each of which analyzes about one-third of an octave [25, 26]. Substantial signal processing appears to be performed within each lamina, potentially including pitch detection [27, 28]. Frequency discrimination through frequency-dependent patterns of network activity might therefore occur in these laminae. Simultaneous recordings from many interconnected neurons within one lamina would provide an experimental test of this hypothesis.

Neural networks can exhibit emergent computational abilities such as synchronous information transmission, memory, and speech recognition that are not present at the level of individual nerve cells [29–34]. It remains uncertain to what extent such brain functions depend upon a neuron's precise action-potential timing as opposed to its average firing rate [11, 35]. Although our study is specific to the auditory system, it may also provide a more general understanding of the usage of temporal codes for other brain functions.

Acknowledgments

We thank L Abbott for discussion as well as P Kumar and D Ó Maoiléidigh for helpful comments on the manuscript. TR holds a Career Award at the Scientific Interface from the Burroughs Wellcome Fund; AJH is an Investigator of Howard Hughes Medical Institute.

Appendix A. Methods

Random neuronal networks are constructed by assigning to every pair (i, j), $i \neq j$, of neurons a connection from i to j with a low probability c. The average number of connections emerging from an individual neuron accordingly reads $C = c(N-1)$ and equals the average number of a neuron's incoming connections. To each connection from a neuron i to another neuron j we assign a time delay t_{ij} that is drawn randomly between a minimal time $t_{\min}$ and a maximal time $t_{\max}$, $t_{ij} \in [t_{\min}, t_{\max}]$. In our simulations we have employed $t_{\min} = 1.2$ ms and $t_{\max} = 2.8$ ms, a standard deviation $s = 100\,\mu$s for the noise in the phase locking, and a period $T = 2$ ms.

The probability distributions in figure 4(b) show a typical result from one random network. All other numerical results, including mean activity patterns and the statistics of distances between individual trials and mean patterns, have been obtained by averaging over at least 100 different random networks.

We measure the arrival of an action potential at a neuron's soma by the time at which the maximum of the depolarization occurs. Each neuron fires an action potential upon arrival of a signal's first external spike. The initiation of subsequent action potentials requires that two action potentials arrive at the neuron's soma within a time window τ; in our simulations we have employed $\tau = 0.6$ ms. Such a difference between generation of the first spike and later ones could result, for example, from spike adaptation in a neuron. Generation of an action potential is followed by a refractory period for the duration of which we have assumed 1.2 ms.

For simulations of network dynamics we have developed a fast, event-based algorithm that stores the propagating spikes and their arrival times at each neuron. At each step in the algorithm we then compute the earliest subsequent time at which a neuron fires a spike, determine to which neurons that spike propagates as well as the associated arrival times, and appropriately update the list of incoming spikes at those neurons. The mean activity patterns as well as the statistics of the pattern distance of a single trial from a mean pattern have been computed from at least 100 trials for each network realization.

Appendix B. Analytical computation of the mean network activity

What is a neuron's average number B of active connections? Suppose that neuron i has an outward connection to excite neuron j and the spike's travel time is t_{ij}. Assume that neuron i fires at a time $nT+\xi_n$, such that the signal arrives at neuron j at the time $nT+\xi_n+t_{ij}$. For spike initiation at neuron j this time may differ no more than a time τ from the arrival time $(n+1)T+\xi_{n+1}$ of the next external spike there. In other words,

$$\xi_n + t_{ij} \in [T+\xi_{n+1}-\tau,\, T+\xi_{n+1}+\tau] \tag{B.1}$$

or

$$\xi_n - \xi_{n+1} \in [T-t_{ij}-\tau,\, T-t_{ij}+\tau]. \tag{B.2}$$

Because $\xi_n-\xi_{n+1}$ is a stochastic process with zero mean and standard deviation $\sqrt{2}s$, the probability $p(T,t_{ij})$ that equation (B.2) is fulfilled reads

$$p(T,t_{ij}) = \frac{1}{2}\left[\operatorname{erf}\left(\frac{T-t_{ij}+\tau}{2s}\right) - \operatorname{erf}\left(\frac{T-t_{ij}-\tau}{2s}\right)\right]. \tag{B.3}$$

An external spike at neuron j together with an internal spike received from neuron i therefore causes neuron j to fire with a probability $p(T,t_{ij})$. The connection from i to j is active if the number of such spikes associated with L external spikes is at least $L/2$. With a binomial probability of

$$\binom{k}{L} p(T,t_{ij})^k \left[1-p(T,t_{ij})\right]^{L-k}, \tag{B.4}$$

the connection from i to j induces a number k of spikes. For medium and large values of L this probability approaches a Gaussian with mean $Lp(T,t_{ij})$ and variance $Lp(T,t_{ij})[1-p(T,t_{ij})]$. The probability $q(T,t_{ij})$ of having at least $L/2$ external spikes then follows from the corresponding cumulative probability distribution and reads

$$q(T,t_{ij}) = \frac{1}{2}\left\{1+\operatorname{erf}\left[\frac{p(T,t_{ij})-1/2}{\sqrt{2p(T,t_{ij})[1-p(T,t_{ij})]/L}}\right]\right\}. \tag{B.5}$$

Denote the index set of neurons that have a forward connection to neuron j as $\mathcal{I}_j$. The average number B of a neuron's active connections then follows as

$$\begin{aligned} B &= \frac{1}{N}\sum_{j=1}^{N}\sum_{i\in\mathcal{I}_j} q(T,t_{ij}) \\ &= \frac{C}{t_{\max}-t_{\min}}\int_{t_{\min}}^{t_{\max}} dt\, q(T,t). \end{aligned} \tag{B.6}$$

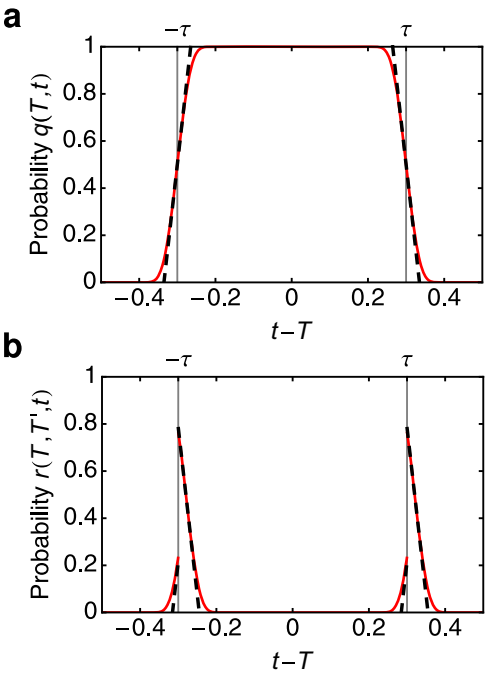

Figure B.1. The probabilities $q(T, t)$ and $r(T, T', t)$ and their linear approximations. (a) The probability $q(T, t)$ (red) is approximately one for $t - T$ between $-\tau$ and τ and zero outside this interval. The transitions at $-\tau$ and τ (gray lines) sharpen for greater signal length; here we have employed $L = 10$. The piecewise-linear approximation $q\,\mathrm{lin}(T, t)$, equation (C.13), is shown as a black dashed line. (b) The probability $r(T, T', t)$ (red) and its piecewise-linear approximation $r_{\mathrm{lin}}(T, T', t)$ (black dashed) are nonzero in only a small interval of $t - T$ around $-\tau$ and τ (gray lines). The curves have been obtained from $L = 10$ and $T' = 1.02\,T$.

When $t_{\min} < T - \tau$ and $T + \tau < t_{\max}$ the integral in the above equation equals approximately 2τ and we obtain

$$B = \frac{2\tau C}{t_{\max} - t_{\min}}. \tag{B.7}$$

In conjunction with equation (3), this relation yields an analytical dependence of the fraction a of active nodes on the connectivity C. This dependence is shown as a black line in figure 3(b) and agrees excellently with numerical results. We find that $a = 0.5$ for a connectivity of $C_* \approx 1.85$.

Appendix C. Analytical computation of pattern distances

As described in the introduction, we quantify the distance between two network activity patterns $\boldsymbol{x} = (x^{(1)}, x^{(2)}, \ldots, x^{(N)})$ and $\boldsymbol{y} = (y^{(1)}, y^{(2)}, \ldots, y^{(N)})$ through the relative Hamming distance

$$d(\boldsymbol{x}, \boldsymbol{y}) = \frac{1}{N} \sum_{i=1}^{N} |x^{(i)} - y^{(i)}|. \tag{C.1}$$

Distinct patterns of network activity result from differences in the active connections. Denote by $\Delta B(\boldsymbol{x}, \boldsymbol{y})$ the average number of a neuron's active connections that differ between the two patterns $\boldsymbol{x}$ and $\boldsymbol{y}$. If this difference is small, as it is for the small differences in the signal period that we consider, the pattern distance $d(\boldsymbol{x}, \boldsymbol{y})$ can be approximated as depending linearly on the difference $\Delta B(\boldsymbol{x}, \boldsymbol{y})$:

$$d(\boldsymbol{x}, \boldsymbol{y}) = \left.\frac{\mathrm{d}a}{\mathrm{d}B}\right|_{B_*} B(\boldsymbol{x}, \boldsymbol{y}), \tag{C.2}$$

in which B_* follows from the network connectivity C_* through equation (B.7).

We start by computing the distance $d(\boldsymbol{X}_T, \boldsymbol{X}_{T'})$ between the mean pattern $\boldsymbol{X}_T$ at period T and the mean pattern $\boldsymbol{X}_{T'}$ at period T'. Consider a connection from a neuron i to another neuron j with a time delay t_{ij}. For the mean patterns we can ignore the phase noise in equation (B.1): the connection is thus active under a signal period T when $T - \tau < t_{ij} < T + \tau$ and vanishes otherwise. Analogously a signal period T' yields an active connection when $T' - \tau < t_{ij} < T' + \tau$ and an inactive connection otherwise. Assume that $T < T'$; the other case follows by analogy. Only when the time delay t_{ij} lies in the intervals $(T - \tau, T' - \tau)$ or $(T + \tau, T' + \tau)$ does the connection then differ in its activity between the two patterns, and the probability to have such a time delay is $2|T - T'|/(t_{\max} - t_{\min})$. The average number $\Delta B(\boldsymbol{X}_T, \boldsymbol{X}_{T'})$ of a neuron's active connections that differ between the two patterns follows as

$$\Delta B(\boldsymbol{X}_T, \boldsymbol{X}_{T'}) = \frac{2C_*}{t_{\max} - t_{\min}} |T' - T| \tag{C.3}$$

and the pattern distance reads

$$d(\boldsymbol{X}_T, \boldsymbol{X}_{T'}) = \left.\frac{\mathrm{d}a}{\mathrm{d}B}\right|_{B_*} \frac{2C_*}{t_{\max} - t_{\min}} |T' - T|. \tag{C.4}$$

As observed numerically, the pattern distance increases linearly in $|T' - T|$ (figure 4(a)). For the parameters employed in our simulations, the above expression yields a slope that is comparable to but about 20% greater than the numerical value.

Let us now compute the distance $d(\boldsymbol{x}_T, \boldsymbol{X}_{T'})$ between a single-trial pattern $\boldsymbol{x}_T$ during period T and the mean pattern $\boldsymbol{X}_{T'}$ during another period T'. This distance varies from trial to trial (figure 4(b)). Again, we consider a connection from a neuron i to another neuron j that induces a certain time delay t_{ij}. As before, the mean pattern $\boldsymbol{X}_{T'}$ is unaffected by the phase noise: the connection is active when $T' - \tau < t_{ij} < T' + \tau$ and vanishes otherwise. For the single-trial pattern $\boldsymbol{x}_T$, however, the activity may fluctuate: as computed above, the connection is active with probability $q(T, t_{ij})$ and zero otherwise (equation (B.5)). To capture this stochasticity we introduce a random binary variable Z_{ij} that is one when the connection from neuron i to neuron j differs in its activity between the single-trial pattern $\boldsymbol{x}_T$ and the mean pattern $\boldsymbol{X}_{T'}$; otherwise Z_{ij} is zero. We find that $Z_{ij} = 1$ with a probability $r(T, T', t_{ij})$ and $Z_{ij} = 0$ with a probability $1 - r(T, T', t_{ij})$ in which

$$r(T, T', t_{ij}) = \begin{cases} q(T, t_{ij}) & \text{if} \quad t_{ij} < T' - \tau \quad \text{or} \quad t_{ij} > T' + \tau, \\ 1 - q(T, t_{ij}) & \text{if} \quad T' - \tau < t_{ij} < T' + \tau. \end{cases} \tag{C.5}$$

Because the difference $\Delta B(\boldsymbol{x}_T, \boldsymbol{X}_{T'})$ follows as the sum over many independent random variables Z_{ij},

$$\Delta B(\boldsymbol{x}_T, \boldsymbol{X}_{T'}) = \frac{1}{N} \sum_{j=1}^{N} \sum_{i \in \mathcal{I}_j} Z_{ij}, \tag{C.6}$$

the central limit theorem guarantees that, in the limit of a large system size N, the distribution of $\Delta B(\boldsymbol{x}_T, \boldsymbol{X}_{T'})$, and hence of the pattern distance $d(\boldsymbol{x}_T, \boldsymbol{X}_{T'})$, approaches a Gaussian distribution (figure 4(b)). The mean value for the distribution of $\Delta B(\boldsymbol{x}_T, \boldsymbol{X}_{T'})$ reads

$$\langle \Delta B(\boldsymbol{x}_T, \boldsymbol{X}_{T'}) \rangle = \frac{1}{N} \sum_{j=1}^{N} \sum_{i \in \mathcal{I}_j} r(T, T', t_{ij}) \tag{C.7}$$

and its variance is

$$\begin{aligned} \left\langle \Delta B(\boldsymbol{x}_T, \boldsymbol{X}_{T'})^2 - \langle \Delta B(\boldsymbol{x}_T, \boldsymbol{X}_{T'}) \rangle^2 \right\rangle &= \frac{1}{N^2} \sum_{j=1}^{N} \sum_{i \in \mathcal{I}_j} r(T, T', t_{ij})[1 - r(T, T', t_{ij})] \\ &= \frac{1}{N^2} \sum_{j=1}^{N} \sum_{i \in \mathcal{I}_j} q(T, t_{ij})[1 - q(T, t_{ij})]. \end{aligned} \tag{C.8}$$

The mean pattern distance follows from equation (C.2) as

$$D(\boldsymbol{x}_T, \boldsymbol{X}_{T'}) = \left. \frac{\mathrm{d}a}{\mathrm{d}B} \right|_{B_*} \frac{1}{N} \sum_{j=1}^{N} \sum_{i \in \mathcal{I}_j} r(T, T', t_{ij}) \tag{C.9}$$

and its variance σ^2 as

$$\sigma^2 = \left(\left. \frac{\mathrm{d}a}{\mathrm{d}B} \right|_{B_*} \right)^2 \frac{1}{N^2} \sum_{j=1}^{N} \sum_{i \in \mathcal{I}_j} q(T, t_{ij})[1 - q(T, t_{ij})]. \tag{C.10}$$

The last equality shows that the variance does not depend on T'. We show that it is also independent of T as long as T is slightly greater than $t_{\min} + \tau$ and less than $t_{\max} + \tau$.

Because the delays t_{ij} are chosen randomly from the interval $[t_{\min}, t_{\max}]$ the sums in equations (C.9) and (C.10) can be expressed through integrals over time delays t between $t_{\min}$ and $t_{\max}$:

$$D(\boldsymbol{x}_T, \boldsymbol{X}_{T'}) = \left. \frac{\mathrm{d}a}{\mathrm{d}B} \right|_{B_*} \frac{C_*}{t_{\max} - t_{\min}} \int_{t_{\min}}^{t_{\max}} r(T, T', t) \tag{C.11}$$

and

$$\sigma^2 = \left(\left. \frac{\mathrm{d}a}{\mathrm{d}B} \right|_{B_*} \right)^2 \frac{C_*}{N(t_{\max} - t_{\min})} \int_{t_{\min}}^{t_{\max}} q(T, t)[1 - q(T, t)]\,. \tag{C.12}$$

To compute the integral in equation (C.12) we employ a piecewise-linear approximation $q_{\mathrm{lin}}(T, t)$ of $q(T, t)$ (figure B.1):

$$q_{\mathrm{lin}}(T, t) = \begin{cases} 0 & \text{if} \quad t < T - \tau - \pi s/\sqrt{2L} \\ & \quad \text{or} \quad t > T + \tau + \pi s/\sqrt{2L}, \\ \frac{1}{2} + \frac{\sqrt{L}}{\sqrt{2}\pi s}(t - T + \tau) & \text{if} \quad T - \tau - \pi s/\sqrt{2L} < t < T - \tau + \pi s/\sqrt{2L}, \\ 1 & \text{if} \quad T - \tau + \pi s/\sqrt{2L} < t < T + \tau - \pi s/\sqrt{2L}, \\ \frac{1}{2} - \frac{\sqrt{L}}{\sqrt{2}\pi s}(t - T + \tau) & \text{if} \quad T + \tau - \pi s/\sqrt{2L} < t < T + \tau + \pi s/\sqrt{2L}. \end{cases} \tag{C.13}$$

The integral then follows as

$$\int_{t_{\min}}^{t_{\max}} q_{\mathrm{lin}}(T,t)\,[1-q_{\mathrm{lin}}(T;t)] = \frac{\sqrt{2}\pi s}{3\sqrt{L}} \tag{C.14}$$

and we obtain

$$\sigma^2 = \left(\left.\frac{\mathrm{d}a}{\mathrm{d}B}\right|_{B_*}\right)^2 \frac{\sqrt{2}\pi s C_*}{3\sqrt{L}N(t_{\max}-t_{\min})}. \tag{C.15}$$

The standard deviation σ therefore decreases as $N^{-1/2}$ with an increasing system size N and as $L^{-1/4}$ for greater signal length L, in agreement with our numerical results (figures 4(c) and 6(a)). The standard deviation is moreover independent of the signal periods T and T' as we have also found numerically (figures 4(b) and 5). The values predicted by the above analytical expression are about 30% lower than those calculated numerically.

The linear approximation $q_{\mathrm{lin}}(T,t)$ results, through equation (C.5), in a piecewise-linear approximation $r_{\mathrm{lin}}(T,T',t)$ for $r(T,T',t)$ that we employ to approximate the integral in equation (C.11) (figure B.1). Two cases then emerge. Firstly, for small period differences $|T'-T| \leqslant \pi s/\sqrt{2L}$ we obtain

$$\int_{t_{\min}}^{t_{\max}} r_{\mathrm{lin}}(T,T',t) = \frac{\pi^2 s^2 + 2L(T'-T)^2}{\sqrt{2L}\pi s} \tag{C.16}$$

and a mean pattern distance of

$$D(\boldsymbol{x}_T, \boldsymbol{X}_{T'}) = \left.\frac{\mathrm{d}a}{\mathrm{d}B}\right|_{B_*} C_* \frac{\pi^2 s^2 + 2L(T'-T)^2}{\sqrt{2L}\pi s(t_{\max}-t_{\min})}. \tag{C.17}$$

The pattern distance is quadratic in $T'-T$ for these small period differences, and has a nonvanishing minimum at $T'=T$ as seen in numerics (figure 5).

Secondly, for larger period differences $|T'-T| \geqslant \pi s/\sqrt{2L}$ we compute

$$\int_{t_{\min}}^{t_{\max}} r_{\mathrm{lin}}(T,T',t) = 2|T'-T| \tag{C.18}$$

and obtain

$$D(\boldsymbol{x}_T, \boldsymbol{X}_{T'}) = \left.\frac{\mathrm{d}a}{\mathrm{d}B}\right|_{B_*} \frac{2C_*}{t_{\max}-t_{\min}}|T'-T|. \tag{C.19}$$

For these larger period differences the pattern distance thus increases linearly in $|T'-T|$ as we have already found numerically (figure 5). Because the value $\Delta T = \pi s/\sqrt{2L}$ separates the two regimes, we consider it to be the network's threshold for period discrimination. The above analytical expression shows that ΔT is independent of the system size N but decreases according to $L^{-1/2}$ with increasing signal length L, in agreement with our numerical results (figure 6(b)).

Equations (C.17) and (C.19) show that the mean distance $D(\boldsymbol{x}_T, \boldsymbol{X}_{T'})$ is invariant under exchange of T and T': $D(\boldsymbol{x}_T, \boldsymbol{X}_{T'}) = D(\boldsymbol{x}_{T'}, \boldsymbol{X}_T)$, in agreement with the numerical results. Because the standard deviation σ does not depend on either T or T', it follows that the distributions of $d(\boldsymbol{x}_T, \boldsymbol{X}_{T'})$ and $d(\boldsymbol{x}_{T'}, \boldsymbol{X}_T)$ are identical.

References

[1] Ulfendahl M 1997 Mechanical responses of the mammalian cochlea *Prog. Neurobiol.* **53** 331–80
[2] Robles L and Ruggero M A 2001 Mechanics of the mammalian cochlea *Physiol. Rev.* **81** 1305–52
[3] Pickles J O 1996 *An Introduction to the Physiology of Hearing* 5th edn (San Diego, CA: Academic)
[4] Hudspeth A J 2008 Making an effort to listen: mechanical amplification in the ear *Neuron* **59** 530–45
[5] Moser T, Neef A and Khimich D 2006 Mechanisms underlying the temporal precision of sound coding at the inner hair cell ribbon synapse *J. Physiol.* **576** 55–62
[6] Oertel D 1997 Encoding of timing in the brain stem auditory nuclei of vertebrates *Neuron* **19** 959–62
[7] Joris P X and Smith P H 2008 The volley theory and the spherical cell puzzle *Neuroscience* **154** 65–76
[8] Köppl C 1997 Phase locking to high frequencies in the auditory nerve and cochlear nucleus magnocellularis of the barn owl, *Tyto alba J. Neurosci.* **17** 3312–21
[9] Köppl C 2009 Evolution of sound localisation in land vertebrates *Curr. Biol.* **19** R635
[10] Grothe B, Pecka M and McAlpine D 2010 Mechanisms of sound localization in mammals *Physiol. Rev.* **90** 983–1012
[11] Rieke F, Warland D, de Ruyter van Stevenick R and Bialek W 1999 *Spikes* (Cambridge, MA: MIT Press)
[12] Lass Y and Abeles M 1975 Transmission of information by the axon. I: noise and memory in the myelinated nerve fiber of the frog *Biol. Cybern.* **19** 61–7
[13] Stuart G, Spruston N and Häusser M 2008 *Dendrites* 1st edn (Oxford: Oxford University Press)
[14] Moore B C 2008 The role of temporal fine structure processing in pitch perception, masking and speech perception for normal-hearing and hearing-impaired people *J. Assoc. Res. Otolaryngol.* **9** 399–406
[15] Sek A and Moore B C J 1994 Frequency discrimination as a function of frequency, measured in several ways *J. Acoust. Soc. Am.* **97** 2479
[16] Moore B C J and Sek A 1995 Effects of carrier frequency, modulation rate and modulation waveform on the detection of modulation and the discrimination of modulation type (amplitude modulation versus frequency modulation) *J. Acoust. Soc. Am.* **97** 2468–78
[17] Moore B C J, Glasberg B R and Flanagan H J 2006 Frequency discrimination of complex tones; assessing the role of component resolvability and temporal fine structure *J. Acoust. Soc. Am.* **119** 480–90
[18] Reichenbach T and Hudspeth A J 2012 Discrimination of low-frequency tones employs temporal fine structure *PLoS ONE* **7** e45579
[19] Licklider J C R 1959 Three auditory theories *Psychology, A Study of Science* ed S Koch (New York: McGraw-Hill) pp 41–144
[20] Srulovicz P and Goldstein J L 1983 A central spectrum model: a synthesis of auditory-nerve timing and place cues in monaural communication of frequency spectrum *J. Acoust. Soc. Am.* **73** 1266–77
[21] Hanekom J J and Krüger J J 2001 A model for frequency discrimination with optimal processing of auditory nerve spike intervals *Hear. Res.* **151** 188–204
[22] Flandrin P 1999 *Time–Frequency/Time-Scale Analysis* 2nd edn (San Diego, CA: Academic)
[23] Faisal A A and Laughlin S B 2007 Stochastic simulations on the reliability of action potential propagation in thin axons *PLoS Comput. Biol.* **3** e79
[24] Sabatini B L and Regehr W G 1996 Timing of neurotransmission at fast synapses in the mammalian brain *Nature* **384** 170–2
[25] Winer J A and Schreiner C E 2004 *The Inferior Colliculus* (Berlin: Springer)
[26] Schreiner C E and Langner G 1997 Laminar fine structure of frequency organization in auditory midbrain *Nature* **338** 383–6
[27] Braun M 1999 Auditory midbrain laminar structure appears adapted to f_0 extraction: further evidence and implications of the double critical bandwidth *Hear. Res.* **129** 71–82
[28] Braun M 2000 Inferior colliculus as candidate for pitch extraction: multiple support from statistics of bilateral spontaneous otoacoustic emissions *Hear. Res.* **145** 130–40

[29] Hopfield J J 1982 Neural networks and physical systems with emergent collective computational abilities *Proc. Natl Acad. Sci. USA* **79** 2554–8
[30] Abeles M 1991 *Corticonics: Neural Circuits of the Cerebral Cortex* (Cambridge: Cambridge University Press)
[31] Anthony M and Bartlett P L 1999 *Neural Network Learning: Theoretical Foundations* (Cambridge: Cambridge University Press)
[32] Vogels T P, Rajan K and Abbott L F 2005 Neural network dynamics *Annu. Rev. Neurosci.* **28** 357–76
[33] Hopfield J J 2004 Encoding for computation: recognizing brief dynamical patterns by exploiting effects of weak rhythms on action-potential timing *Proc. Natl Acad. Sci. USA* **101** 6255–60
[34] Gütig R and Sompolinsky H 2009 Time-warp-invariant neuronal processing *PLoS Biol.* **7** e1000141
[35] Perkel D H and Bullock T H 1968 Neural coding *Neurosci. Res. Prog. Bull.* **6** 221–348